NANO LETTERS

2009
Vol. 9, No. 6
2423-2426

Near-Degenerate Four-Wave-Mixing Microscopy

Wei Min,† Sijia Lu,† Markus Rueckel, Gary R. Holtom, and X. Sunney Xie*

Department of Chemistry and Chemical Biology, Harvard University, Cambridge, Massachusetts 02138

Received April 6, 2009

ABSTRACT

Fluorescence microscopy has been widely used to explore the nanoscale world because of its superb sensitivity, but it is limited to fluorescent samples. Hence, various spectroscopic contrasts have been explored for imaging nonfluorescent species. Here we report a multiphoton microscopy based on single-beam near-degenerate four wave mixing (ND-FWM), by detecting a coherent signal generated by the sample at frequencies close to the "edge" of the spectrally "truncated" incident femtosecond pulses. ND-FWM microscopy allows label-free biomedical imaging with high sensitivity and spatial resolution. In particular, by achieving a nearly perfect phase matching condition, ND-FWM generates almost the highest nonlinear coherent signal in a bulk medium and provides a contrast mechanism different from other nonlinear imaging techniques. More importantly, we developed an electronic resonant version of ND-FWM for absorbing but nonfluorescent molecules. Ultrasensitive chromophore detection (~50 molecules) and hemoglobin imaging are demonstrated, by harnessing a fully (triply) resonant enhancement of the nonlinear polarization and using optical heterodyne detection.

Nonlinear coherent spectroscopies,[1,2] such as coherent anti-Stokes Raman scattering (CARS),[3,4] second harmonic generation (SHG),[5,6] third harmonic generation (THG),[7,8] two-photon resonance enhanced stimulated parametric emission,[9] and self-phase modulation,[10] offer various powerful contrast mechanisms for label-free detection and imaging of nonfluorescent objects. First, nonlinear coherent spectroscopies offer intrinsic three-dimensional (3D) optical sectioning, as in two-photon fluorescence microscopy.[11] Second, the nonlinear wave mixing often generates a signal at a color different from those of the incident lasers, creating a nearly background-free situation. Third, coherent amplification could occur due to constructive interference among the nonlinear induced dipoles.

However, a few limitations still exist for the current nonlinear coherent microscopies. In particular, one or more virtual states are often involved in the underlying optical transitions, which limits the efficiency of nonlinear signal generation. Besides, symmetry and phase matching condition often limit the harmonic generation microscopies. For example, SHG only works for noncentrosymmetric materials,[5,6] while THG only arises from interfaces or small inclusions because of the large phase mismatch associated with Guoy phase shift near focus.[7,8,12−14] In addition, two (or more) synchronized ultrafast lasers[3,9] or complex spectral phase modulation[4,10] is sometimes required, which increases the instrumental complexity.

Here we introduce single-beam near-degenerate four wave mixing (ND-FWM) as a imaging contrast mechanism, by detecting a coherent signal generated by the sample at frequencies close to the "edge" of the spectrally "truncated" incident broad band femtosecond pulses. As shown in Figure 1, the high-frequency portion of the broad band Ti−Sa laser is sharply blocked by a 4-f pulse-shaper[15] in its Fourier domain. After the sample was excited with such a spectrally truncated pulse, the ND-FWM signal is generated at new frequencies close to the spectral "cut edge". Hence, unlike the strictly degenerate FWM, ND-FWM involves similar but not identical input frequencies, and the generated signal can be spectrally separated from the incident light, creating a nearly background-free situation. This microscopy uses a single femtosecond laser for excitation, and a high bandwidth intensity-based detector and, most importantly, is readily suitable for nonfluorescent chromophore imaging through triple resonance.

Theoretically the general FWM arises from a third-order nonlinear interaction of four coherent optical fields with the material. The general form of the induced polarization at frequency ω_4 can be written as[2]

$$P_i^{(3)}(\omega_4 = \pm\omega_1 \pm \omega_2 \pm \omega_3) \propto \sum_{jkl} \sum_{(1,2,3)} \chi_{ijkl}^{(3)}(-\omega_4;\pm\omega_1,\pm\omega_2,\pm\omega_3)E_j(\omega_1)E_k(\omega_2)E_l(\omega_3) \quad (1)$$

which describes a coupling between four waves through the nonlinear susceptibility tensor $\chi_{ijkl}^{(3)}$. The notation $\sum_{(1,2,3)}$ requires the relation $\omega_4 = \pm\omega_1 \pm \omega_2 \pm \omega_3$ to be held in

* Corresponding author, xie@chemistry.harvard.edu.
† These authors contribute equally to this work.

10.1021/nl901101g CCC: $40.75 © 2009 American Chemical Society
Published on Web 05/11/2009

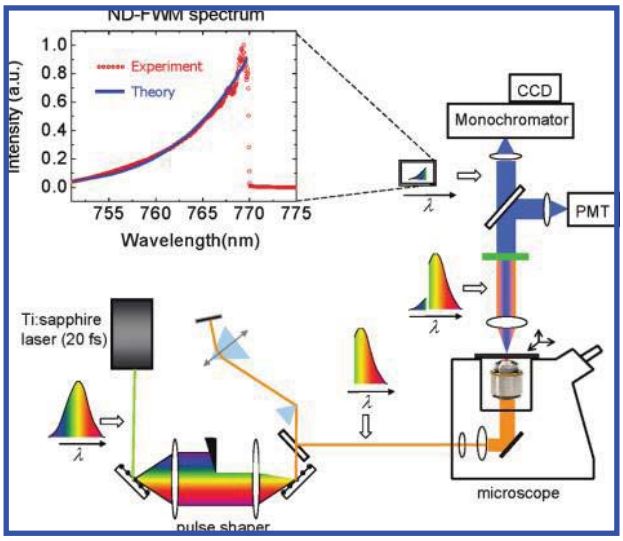

Figure 1. Experimental apparatus of ND-FWM spectroscopy and microscopy. The light spectra at various propagating stages (after the laser output, after the 4-f pulse shaper but before the microscope, immediately after the sample, after the optical filter but in front of the detector) are illustrated individually. Monochromator/CCD and PMT detector are equipped for spectroscopy and microscopy mode, respectively. The generated ND-FWM spectrum from glass is measured and compared with theoretical prediction from eq 3. Technical details are described in the Supporting Information.

performing the summation. The frequency values of photons that are destroyed in the nonlinear process are written with positive signs, while the created frequencies with negative signs. $\chi_{ijkl}^{(3)}$ for ND-FWM is given by

$$\chi^{(3)}(-\omega_4;\omega_1,-\omega_2,\omega_3) = \frac{N}{\hbar^3}\mathbf{P}_F\sum_{m,l,n}\frac{\mu_{km}\mu_{ml}\mu_{ln}\mu_{nk}}{(\omega_{mk}-\omega_1-i\gamma_{mk})(\omega_{lk}-\omega_1+\omega_2-i\gamma_{lk})(\omega_{nk}-\omega_4-i\gamma_{nk})} \quad (2)$$

where $\mathbf{P}_F$ is the full permutation operator, μ is the transition dipole moment, ω is the energy difference between corresponding energy levels, and γ is the homogeneous line width of the associated electronic or vibrational transition.[2]

The spectrum of ND-FWM can be experimentally measured and theoretically understood. As shown in Figure 1, the recorded ND-FWM spectrum exhibits a characteristic decay in frequency from small frequency shift to large shift, with respect to the incident spectrum. Such a decaying spectrum is due to the fact that, given the incident broad band spectrum, there exist more frequency combinations matching $\omega_4 = \omega_1 - \omega_2 + \omega_3$ for smaller frequency shift than for larger frequency shift. Quantitatively, we can describe the spectrum with a continuous integration as

$$I(\omega_4)d\omega_4 \propto |P^{(3)}(\omega_4=\omega_1-\omega_2+\omega_3)|^2 \propto \left|\int_{-\infty}^{\infty}d\omega_1\int_{-\infty}^{\infty}d\omega_2\int_{-\infty}^{\infty}d\omega_3\chi^{(3)}(-\omega_4;\omega_1,-\omega_2,\omega_3)E(\omega_1)E^*(\omega_2)E(\omega_3)\delta(\omega_4-\omega_1+\omega_2-\omega_3)\right|^2 \quad (3)$$

where the delta function ensures that the triple integration satisfy $\omega_4 = \omega_1 - \omega_2 + \omega_3$. We find that the experimental measurement agrees satisfactorily with the prediction of eq 3 which is numerically computed. Such a rapidly decaying spectrum is precisely the reason why we have to approach the small frequency shifts as closely as possible by means of laser spectral truncation (as close as ~5 nm).

We argue that ND-FWM microscopy might generate the highest nonlinear coherent signal in bulk, providing a contrast mechanism different from CARS, SHG, or THG. It is well-known that coherent signal generation of a general FWM process is only efficient near the phase matching condition.[16] Moreover, Gouy phase shift has been shown to play an important role in nonlinear coherent microscopy, by generating a phase delay, $\boldsymbol{\delta}\mathbf{k}_G$, among the excitation fields along the axial direction of the tight focus. ND-FWM offers two distinct mechanisms in optimizing the phase matching condition. First, by having a near degeneracy, the refractive index can be regarded as nearly invariant within such a narrow frequency range. As a result, $n_4\omega_4 - n_3\omega_3 + n_2\omega_2 - n_1\omega_1 \approx 0$, where n is the refractive index of the material at corresponding frequency ω. Second, $\boldsymbol{\delta}\mathbf{k}_G$ from Guoy phase shift is substantially canceled by the negative contribution from the conjugated field $E^*(\omega_2)$. This nearly perfect phase matching condition leads to a coherence length longer than the focal depth and, therefore, to a nearly complete constructive interference within the whole focal volume from a bulk sample. In contrast, $\boldsymbol{\delta}\mathbf{k}_G$ from three fields in THG are all added up positively, which results in zero THG signal from bulk homogeneous medium under the tight-focusing condition.[7,8,12−14]

ND-FWM microscopy is characterized in Figure 2. The z-scanning profile over water/glass/air (Figure 2a) proves that this technique is bulk sensitive instead of interface sensitive. This is predicted by the above theoretical discussion on the nearly perfect phase matching condition of ND-FWM microscopy. In contrast, SHG and THG signals would only arise at the interface but not inside the water or glass. As a simple demonstration, Figure 2b shows the image of polystyrene beads (diameter of 600 nm) dispersed on the glass surface. Meanwhile, a control image (Figure 2c) on the same area is taken when the excitation pulse width is stretched by tuning the prism pair pulse compressor. The fact that the image contrast almost vanishes for the longer pulse width supports that the signal in Figure 2b is indeed from the nonlinear process instead of the linear refractive index variation. The measured lateral full width at half-maximum for the 50 nm bead is about 260 nm, which is better than the one-photon confocal resolution of 290 nm calculated as $0.61\lambda/1.4\text{NA}$ ($\lambda \sim 800$ nm), due to the third-order intensity dependence. Visible light (e.g., 500 nm) would allow resolution even sharper than 150 nm, made possible by the near degeneracy between excitation and detection. We note that this cannot be achieved by THG microscopy.

ND-FWM offers a useful contrast mechanism for imaging biological samples without exogenous labels, since $\chi_{ijkl}^{(3)}$ could range from 10^{-8} to 10^{-15} cm^2/W,[2,12] and is highly sensitive to the degree of electron delocalization. The mammalian cell image (Figure 2d) identifies the subcellular organelles such as nucleus and mitochondria. The characteristic fiber morphology as well as cigar-shaped multinucleate cells is clearly visible in the muscle tissue image (Figure 2e). The brain image shows fiber tracts in the corpus callosum (Figure 2f).

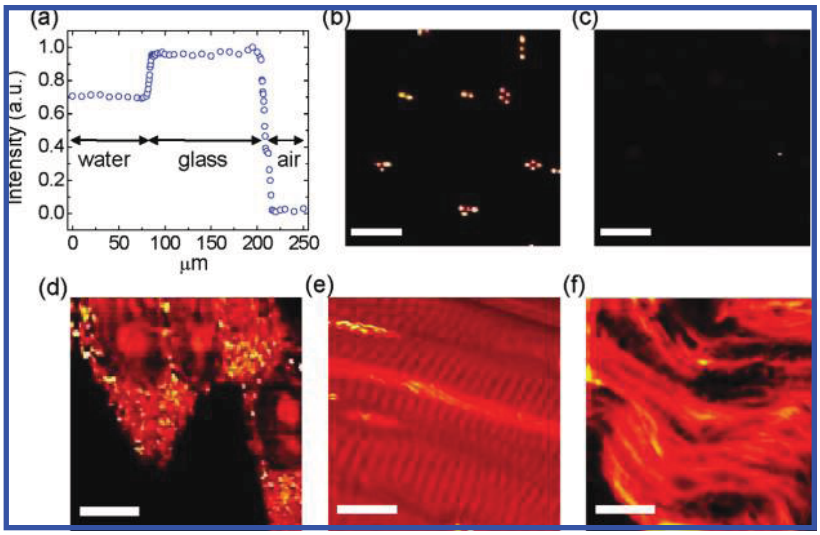

Figure 2. Live cell and tissue imaging with ND-FWM microscopy. (a) The *z*-scanning profile over water/glass/air proves the ND-FWM signal is bulk sensitive instead of interface sensitive. (b) Image of polystyrene beads (d = 600 nm) dispersed on the glass surface. (c) Control image on the same area as (b) but excited with longer excitation pulse width. Images of (b) and (c) demonstrate the nonlinear nature of image contrast. (d) Live human lung cancer cells (cultured A549 cell line). Cellular organelles such as nucleus and mitochondria are clearly visible. Tissue morphology is demonstrated by (e) muscle tissue and (f) brain tissue slices which were freshly cut off from a sacrificed mouse. ~1 mW average laser power was used in (d), (e), and (f). Image rate: 10 s. Scale bar: 10 μm.

We now explore the electronic resonance version of ND-FWM, which would significantly enhance the detection sensitivity and molecular specificity. According to eq 2, a full resonance condition can be achieved when the excitation laser frequency is tuned to resonance with a molecular electronic transition. We emphasize that the resonance enhancement is occurring not only for the excitation frequencies but also for the emission/signal frequencies, because of the near degeneracy. Furthermore, the electronic coupled low-frequency vibronic states are also resonantly excited by the broad-band pulse. Therefore, triple resonance would minimize of all three factors in the denominator of eq 2, thus significantly enhancing the generation efficiency of ND-FWM signal.

Electronic resonant ND-FWM can be utilized for ultrasensitive detection of highly absorbing but nonfluorescent molecular species. In Figure 3, we demonstrate a microspectroscopy application on neocyanine which has an intense absorption (ε ~180000 M^{-1} cm^{-1}) but nondetectable fluorescence in solution due to extremely short excited state lifetime (approximately picoseconds). As shown in Figure 3a, the shaped incident pulse spectrum is tuned to match the absorption peak of neocyanine around 772 nm. Under this resonance condition, the generated ND-FWM signal from neocyanine solution rapidly goes up with increasing concentration (Figure 3b), with a detection sensitivity of about 1 μM in 100 ms integration time. This corresponds to ~50 molecules within the laser focus (whose volume is estimated to be about 10^{-16} L). This represents the highest detection sensitivity of nonlinear coherent microscopy to the best of our knowledge, which is ~5 times better than the recently developed triple-resonance CARS microspectroscopy[17] due to the better resonance condition for emission/signal frequency in ND-FWM. We find that optical heterodyne detection also contributes to such a superb sensitivity, as suggested by the linear concentration dependence shown in Figure 3c. This observed linear concentration dependence at the low concentration limit is due to the interference between the relatively small resonant signal from the low-concentration solute and the strong nonresonant contribution from the ethanol solvent.

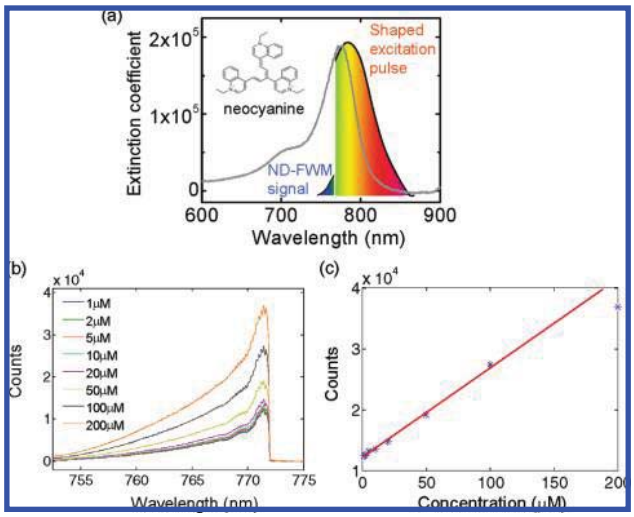

Figure 3. Ultrasensitive detection of absorbing but nonfluorescent molecules with electronic resonant ND-FWM microspectroscopy. (a) Absorption spectrum and molecular structure of neocyanine are shown. The shaped excitation pulse (in red/orange) is resonant with the neocyanine absorption peak (~775 nm). The spectrum of the ND-FWM signal is illustrated in green/blue (<772 nm). (b) ND-FWM spectra for various neocyanine concentrations in ethanol solution. The steep cutoff around 772 nm is due to the rejection from triple-monochromator. ~1 mW average laser power at focus. (c) Concentration dependence of the ND-FWM signal (the peak counts of the spectra shown in (b)). The linear dependence at low concentration indicates an optical heterodyne effect. The detection sensitivity is around 1 μM within 100 ms integration time.

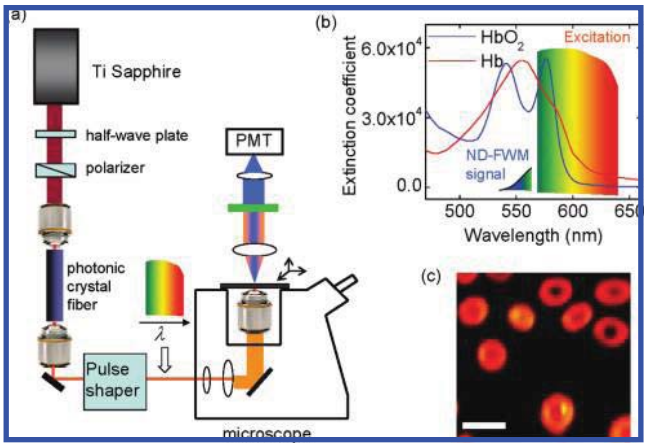

Figure 4. Imaging hemoglobin by electronic resonant ND-FWM microscopy. (a) Experimental apparatus for supercontinuum generation from a photonic crystal fiber. Technical details are described in the Supporting Information. (b) Truncated supercontinuum excitation pulse is resonant with the *Q* band of deoxyhemoglobin (Hb) and oxyhemoglobin (HbO_2) absorption spectra. The spectrum of ND-FWM signal is illustrated in green/blue (<570 nm). (c) Electronic resonant ND-FWM image of red blood cells of a blood smear layer. The donut shape of red blood cells is clearly illustrated. Scale bar: 10 μm.

Finally, in Figure 4, we demonstrate electronic resonant ND-FWM microscopy by imaging nonfluorescent hemoglobin in red blood cells. To be resonant with the *Q* band (~550 nm) of hemoglobin absorption spectrum (Figure 4b), a visible supercontinuum is generated from a photonic crystal fiber with double zero dispersion wavelengths[18] (Figure 4a). Such a supercontinuum is a promising ultrafast coherent source for exciting chromophores in the visible spectrum. The electronic resonant ND-FWM image (Figure 4c) clearly shows the donut shape of red blood cells. We note that our image exhibits much stronger contrast compared with the reported THG images of red blood cells,[19] which could be due to the one-photon electronic resonance employed here.

As a single-beam intensity-based multiphoton imaging modality, ND-FWM microscopy provides a new and easy-to-use nonlinear contrast mechanism based on a bulk-sensitive electronic polarization that is excited and detected most efficiently. This technique not only allows 3D high-resolution imaging of transparent live cells and tissues without labeling but also enables sensitive detection and mapping of biologically important chromophores such as hemoglobin, β-carotene, cytochrome *c*, and rhodopsin.

Acknowledgment. We thank Christian Freudiger and Brain Saar for helpful discussions. This work is supported by NSF (DBI-0649892) and DOE/BES (DE-FG02-07ER15875).

Supporting Information Available: Details of materials and methods, instrumental setup of the microscope, microspectroscopy recording, and supercontinuum generation from a photonic crystal fiber. This material is available free of charge via the Internet at http://pubs.acs.org.

References

(1) Shen, Y. R. *The Principles of Nonlinear Optics.*; John Wiley & Sons Inc.: New York, 1988.
(2) Boyd, R. W. *Nonlinear optics*, 2nd ed.; Academic Press: San Diego, 2003.
(3) Evans, C. L.; Xie, X. S. Coherent anti-Stokes Raman scattering microscopy: chemically selective imaging for biology and medicine. *Annu. Rev. Anal. Chem.* **2008**, *1*, 883–909.
(4) Dudovich, N.; Oron, D.; Silberberg, Y. Single-pulse coherently controlled nonlinear Raman spectroscopy and microscopy. *Nature* **2002**, *418*, 512–514.
(5) Hellwarth, R.; Christensen, P. Nonlinear optical microscopic examination of structure in polycrystalline ZnSe. *Opt. Commun.* **1974**, *12*, 318–322.
(6) Sheppard, C. J. R.; Kompfner, R.; Gannaway, J.; Walsh, D. Scanning harmonic optical microscope. *IEEE J. Quantum Electron.* **1977**, *13E*, 100D.
(7) Barad, Y.; Eisenberg, H.; Horowitz, M.; Silberberg, Y. Nonlinear scanning laser microscopy by third harmonic generation. *Appl. Phys. Lett.* **1997**, *70*, 922–924.
(8) Squier, J. A.; Müller, M.; Brakenhoff, G. J.; Wilson, K. R. Third harmonic generation microscopy. *Opt. Express* **1998**, *3*, 315–324.
(9) Keisuke, I.; et al. Stimulated parametric emission microscopy. *Opt. Express* **2006**, *14*, 786–793.
(10) Fischer, M. C.; Ye, T.; Yurtsever, G.; Miller, A.; Ciocca, M.; Wagner, W.; Warren, W. S. Two-photon absorption and self-phase modulation measurements with shaped femtosecond laser pulses. *Opt. Lett.* **2005**, *30*, 1551.
(11) Denk, W.; Strickler, J.; Webb, W. W. Two-photon laser scanning fluorescence microscopy. *Science* **1990**, *248*, 73.
(12) Débarre, D.; et al. Imaging lipid bodies in cells and tissues using third-harmonic generation microscopy. *Nature Methods* **2006**, *3*, 47–53.
(13) Cheng, J. X.; Xie, X. S. Green's function formulation for third harmonic generation microscopy. *J. Opt. Soc. Am. B* **2002**, *19*, 1604–1610.
(14) Cheng, J. X.; Xie, X. S. Coherent anti-Stokes Raman scattering microscopy: instrumentation, theory and applications. *J. Phys. Chem. B* **2004**, *108*, 827.
(15) Weiner, A. M. Femtosecond pulse shaping using spatial light modulators. *Rev. Sci. Instrum.* **2000**, *71*, 1929–1969.
(16) Potma, E. O.; de Boeij, W. P.; Wiersma, D. A. Nonlinear coherent four- wave mixing in optical microscopy. *J. Opt. Soc. Am. B* **2000**, *17*, 1678–1684.
(17) Min, W.; Lu, S.; Holtom, G. R.; Xie, X. S. Triple-resonance coherent anti-Stokes Raman scattering micro-spectroscopy. *ChemPhysChem* **2009**, *10*, 344–347.
(18) Murugkar, S.; Brideau, C.; Ridsdale, A.; Naji, M.; Stys, P. K.; Anis, H. Coherent anti-Stokes Raman scattering microscopy using photonic crystal fiber with two closely lying zero dispersion wavelengths. *Opt. Express* **2007**, *15*, 14028–14037.
(19) Clay, G. O.; et al. Spectroscopy of third-harmonic generation: evidence for resonances in model compounds and ligated hemoglobin. *J. Opt. Soc. Am. B* **2006**, *23*, 932–950.

NL901101G